STRUCTURAL SCIENCE CRYSTAL ENGINEERING MATERIALS
ISSN 2052-5206

Variable-temperature single-crystal X-ray diffraction study of tetragonal and cubic perovskite-type barium titanate phases

Tomotaka Nakatani,[a]* Akira Yoshiasa,[a] Akihiko Nakatsuka,[b] Tatsuya Hiratoko,[a] Tsutomu Mashimo,[a] Maki Okube[c] and Satoshi Sasaki[c]

[a]Graduate School of Sciences and Technology, Kumamoto University, 2-39-1 Kurokami, Kumamoto 860-8555, Japan, [b]Graduate School of Science and Engineering, Yamaguchi University, Ube, Yamaguchi 755-8611, Japan, and [c]Materials and Structures Laboratory, Tokyo Institute of Technology, Yokohama 226-850, Japan. *Correspondence e-mail: nakatani@spring8.or.jp

Received 12 March 2015
Accepted 25 November 2015

Edited by N. B. Bolotina, Russian Academy of Sciences, Russia

Keywords: perovskite; high temperature; $BaTiO_3$; ferroelectricity; X-ray diffraction.

CCDC references: 1438856; 1438857; 1438858; 1438859; 1438860; 1438861; 1438862; 1438863; 1438864; 1438865; 1438866; 1438867; 1438868; 1438869; 1438870; 1438871; 1438872; 1438873; 1438874

Supporting information: this article has supporting information at journals.iucr.org/b

A variable-temperature single-crystal X-ray diffraction study of a synthetic $BaTiO_3$ perovskite has been performed over the temperature range 298–778 K. A transition from a tetragonal ($P4mm$) to a cubic ($Pm\bar{3}m$) phase has been revealed near 413 K. In the non-centrosymmetric $P4mm$ symmetry group, both Ti and O atoms are displaced along the c-axis in opposite directions with regard to the Ba position fixed at the origin, so that Ti^{4+} and Ba^{2+} cations occupy off-center positions in the TiO_6 and BaO_{12} polyhedra, respectively. Smooth temperature-dependent changes of the atomic coordinates become discontinuous with the phase transition. Our observations imply that the cations remain off-center even in the high-temperature cubic phase. The temperature dependence of the mean-square displacements of Ti in the cubic phase includes a significant static component which means that Ti atoms are statistically distributed in the off-center positions.

1. Introduction

The $BaTiO_3$ perovskite has been intensively studied owing to its excellent ferroelectric properties at ambient conditions. Its tetragonal phase, which is stable at ambient conditions, undergoes a phase transition to orthorhombic at 268 K and to rhombohedral at 183 K. These three phases are polar and ferroelectric (Evans, 1961).

The tetragonal room-temperature phase was originally assigned to the space group $P4/mmm$ (Megaw, 1945, 1946, 1947). Subsequently, it has been confirmed from convergent-beam electron diffraction (Tanaka & Lehmpfuhl, 1972) that its actual symmetry group is $P4mm$, which has also been indicated by other techniques (Rhodes, 1949; Evans, 1951; Frazer *et al.*, 1955; Danner *et al.*, 1960; Harada *et al.*, 1970). The symmetry reduction from $Pm\bar{3}m$ (cubic) to $P4mm$ (tetragonal) involves a slight contraction of the a axis and an extension of the c axis. Three crystallographically equivalent O atoms in the cubic structure separate into one O1 atom at the center of the (001) face of the tetragonal cell, and two symmetry-related O2 atoms at the centers of the (100) and (010) faces. The Ti, O1 and O2 atoms are displaced parallel to the c axis forming two unequal Ti—O1 and four equal Ti—O2 distances. Although deviations from the ideal atomic radii facilitate this reorganization, atomic size is unlikely to be the driving force because it would involve antisymmetric displacements of O1 atoms arising from an essentially symmetric crystal field (Buttner & Maslen, 1992).

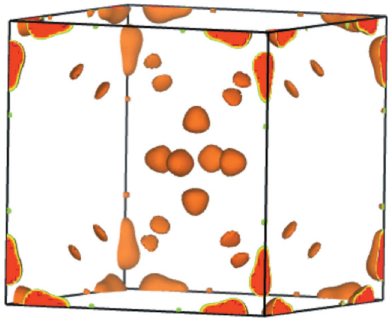

Temperature-dependent crystal structure analysis is necessary to understand the detailed ferroelectric mechanism of $BaTiO_3$ perovskite. The spontaneous polarization of the tetragonal phase is caused by the displacement of positive and negative ions in opposite directions. The spontaneous polarization decreases with increasing temperature and disappears above the Curie point (T_c) of 393 K with the structural phase transition to the cubic phase ($Pm\overline{3}m$). Consequently, the $BaTiO_3$ loses ferroelectricity at this temperature. This type of phase transition is called the ferroelectric phase transition or dielectric ferroelectric phase transition.

The ferroelectricity of perovskites is generated by permanent dipole moments originating from the displacements of cations and anions from their equilibrium positions in opposite directions. Ferroelectric phase transitions are often characterized as either displacement type or order–disorder type, although some phase transitions include both behaviors. The former type has the transition mechanism that cations and anions return to equilibrium positions at the ferroelectric phase transition point, and thereby dipole moments disappear. Meanwhile, the latter type has the transition mechanism that the dipole moments in each unit cell begin to be rearranged in random directions at the ferroelectric transition point so that they are disordered with the completion of the ferroelectric transition at higher temperature. The ferroelectric transition of $BaTiO_3$ is considered to be of the displacement type and its ferroelectricity has mainly been discussed based only on the displacement of the Ti ion from its central position in the TiO_6 octahedron. However, recent X-ray absorption fine-structure (XAFS) studies have proposed that it includes both characters of the order–disorder type and displacement type (Sicron *et al.*, 1994; Ravel & Stern, 1995; Revel *et al.*, 1998; Miyanaga *et al.*, 2002). If the ferroelectric transition has partial order–disorder character, the local distortion around the Ti atom will be able to remain in the cubic phase. Clarifying whether or not the ferroelectric phase transition of $BaTiO_3$ includes the character of the order–disorder type is important for the elucidation of its transition mechanism.

Single-crystal structure studies of $BaTiO_3$ were previously carried out only at room temperature using X-ray diffraction (Buttner & Maslen, 1992; Harada *et al.*, 1970) and neutron diffraction (Harada *et al.*, 1970), and the static configurational displacement of each atom in the tetragonal phase was not observed. Many models of the phase-transition mechanism and ferroelectricity in $BaTiO_3$ polymorphs have been proposed using various techniques (Comès *et al.*, 1968, 1970; Itoh *et al.*, 1985; Tkacz-Śmiech *et al.*, 2003). The statistical distribution of not only Ti but also Ba, even in the low temperature phases, was adopted by almost all models. In the tetragonal and cubic phases, the displacement of the Ti atom along the body diagonal of the unit cell constitutes the main trend in the models. These models are inconsistent with previous single-crystal diffraction studies (Buttner & Maslen, 1992; Harada *et al.*, 1970), and require careful consideration. Single-crystal diffraction is one of the most reliable structural investigation methods.

In order to examine the relationship between the structural changes in the tetragonal and cubic phases of $BaTiO_3$ and its ferroelectric phase transition mechanism, we have carried out single-crystal X-ray structure analyses in the wide temperature range 298–778 K. In this study, we have determined the temperature dependence of the mean square displacements for each atom, and of the distortion in the ferroelectric phase. The possibility of Ti displacement from the central position of the TiO_6 octahedron in the cubic phase, which has long been discussed, is assessed together with the mechanism of ferroelectricity.

2. Experiment and analysis

Single crystals of the tetragonal perovskite-type $BaTiO_3$ (99.99%) grown by the Czochralski method were purchased from MtI. Co., Ltd. A single crystal used for X-ray measurements was carefully ground to a sphere 140 (1) μm in diameter and placed into a silica-glass capillary. Intensity data were collected at 19 temperature points in the range 298–778 K using a Rigaku AFC-7R four-circle diffractometer with graphite-monochromated Mo $K\alpha$ radiation (λ = 0.71069 Å) at the operating condition of 60 kV and 200 mA. In the data collections above room temperature, the high temperature was achieved by a continuous flow of N_2 gas heated by an electric resistance heater; thereby the crystal was directly heated. Prior to the data collections, sample temperatures were calibrated using a K-type thermocouple set exactly at the sample position. Temperature fluctuations during the data collections were kept to within ±0.2 K (Nakatsuka *et al.*, 2011).

The unit-cell parameters at each temperature were determined by the least-squares method from a set of 25 reflections within the range $45 \leq 2\theta \leq 50^\circ$. Intensity data were collected within $2 \leq 2\theta \leq 120^\circ$ for each temperature by the continuous ω–2θ scan mode, and consequently reflections between 1124 and 605 were measured for each phase. The intensities of reflections within one quadrant (for tetragonal phases) and one octant (for cubic phases) were measured at a scan speed of 4° min^{-1}. After the corrections for Lorentz–polarization factors and absorption effects, the intensity data were averaged in Laue symmetry $4mm$ and $m\overline{3}m$ to give independent reflections for the tetragonal and cubic phases, respectively. All the measured reflections and all the independent reflections after averaging were observed with $|F_o| \geq 3\sigma(|F_o|)$, and the sets of reflections were employed for the structure refinements. Internal residuals of the equivalent reflections (R_{int}) varied between 0.0085 and 0.0130 for each temperature.

The structure refinements were carried out by minimizing the function $\sum w(|F_o| - |F_c|)^2$ using the full-matrix least-squares program *RADY* (Sasaki, 1987). Scattering factors were taken from *International Tables for Crystallography* (Table 6.1.1.3; Wilson, 1992) for Ba^{2+} and Ti^{4+} and from Tokonami (1965) for O^{2-}. Anomalous dispersion coefficients for each element were also taken from *International Tables for Crystallography* (Table 4.2.6.8; Wilson, 1992). Several correction models for the secondary extinction effects were

Table 1
Experimental details.

T (K)	298	303	323	343	363
Crystal data					
Crystal system, space group	Tetragonal, *P*4*mm*	Tetragonal, *P*4*mm*	Tetragonal, *P*4*mm*	Tetragonal, *P*4*mm*	Tetragonal, *P*4*mm*
a, b, c (Å)	3.9925 (2), 3.9925 (2), 4.0373 (3)	3.9925 (2), 3.9925 (2), 4.0371 (2)	3.9946 (1), 3.9946 (1), 4.0375 (2)	3.9962 (2), 3.9962 (2), 4.0363 (3)	3.9981 (1), 3.9981 (1), 4.0342 (2)
V (Å^3)	64.35 (1)	64.35 (1)	64.43 (1)	64.43 (1)	64.46 (1)
Z	1	1	1	1	1
Radiation type	Mo $K\alpha$	Mo $K\alpha$	Mo $K\alpha$	Mo $K\alpha$	Mo $K\alpha$
μ (mm^{-1})	18.04	18.04	18.17	18.08	18.00
Crystal size (mm)	0.14 (radius)	0.14 (radius)	0.14 (radius)	0.14 (radius)	0.14 (radius)
Data collection					
Diffractometer	Rigaku AFC7R	Rigaku AFC7R	Rigaku AFC7R	Rigaku AFC7R	Rigaku AFC7R
Absorption correction	ψ scan	ψ scan	ψ scan	ψ scan	ψ scan
No. of measured, independent and observed [$F > 3.0\ \sigma(F)$] reflections	1124, 595, 595	1124, 593, 593	1124, 593, 593	1124, 592, 592	1124, 591, 591
R_{int}	0.011	0.008	0.009	0.008	0.029
$2\theta_{max}$ (°)	120	120	120	120	120
$(\sin\theta/\lambda)_{max}$ (Å^{-1})	1.219	1.219	1.219	1.219	1.219
Refinement					
$R[F > 3\sigma(F)]$, $wR(F)$, S	0.009, 0.010, 1.66	0.009, 0.010, 1.21	0.009, 0.011, 1.35	0.012, 0.014, 1.73	0.011, 0.013, 1.59
No. of reflections	595	593	593	592	591
No. of parameters	14	14	14	14	14

T (K)	378	388	398	413	423
Crystal data					
Crystal system, space group	Tetragonal, *P*4*mm*	Tetragonal, *P*4*mm*	Tetragonal, *P*4*mm*	Cubic, $Pm\bar{3}m$	Cubic, $Pm\bar{3}m$
a, b, c (Å)	3.9996 (3), 3.9996 (3), 4.0328 (5)	4.0008 (1), 4.0008 (1), 4.0309 (2)	4.0020 (1), 4.0020 (1), 4.0280 (2)	4.0097 (2), 4.0097 (2), 4.0097 (2)	4.0106 (2), 4.0106 (2), 4.0106 (2)
V (Å^3)	64.51 (1)	64.52 (1)	64.51 (1)	64.47 (1)	64.51 (1)
μ (mm^{-1})	17.93	17.90	17.92	18.05	17.99
Crystal size (mm)	0.14 (radius)	0.14 (radius)	0.14 (radius)	0.14 (radius)	0.14 (radius)
Data collection					
No. of measured, independent and observed [$F > 3.0\ \sigma(F)$] reflections	1124, 533, 533	1124, 582, 582	1124, 524, 524	602, 118, 118	602, 123, 123
R_{int}	0.016	0.013	0.018	0.029	0.023
$2\theta_{max}$ (°)	120	120	120	120	120
$(\sin\theta/\lambda)_{max}$ (Å^{-1})	1.219	1.219	1.219	1.219	1.219
Refinement					
$R[F > 3\sigma(F)]$, $wR(F)$, S	0.017, 0.020, 1.76	0.014, 0.016, 1.68	0.023, 0.027, 1.78	0.022, 0.023, 1.46	0.014, 0.013, 1.32
No. of reflections	533	582	524	118	123
No. of parameters	14	14	14	6	6

T (K)	448	473	498	548	598
Crystal data					
Crystal system, space group	Cubic, $Pm\bar{3}m$	Cubic, $Pm\bar{3}m$	Cubic, $Pm\bar{3}m$	Cubic, $Pm\bar{3}m$	Cubic, $Pm\bar{3}m$
a (Å)	4.0118 (2)	4.0128 (2)	4.0139 (2)	4.0167 (1)	4.0191 (1)
V (Å^3)	64.57 (2)	64.62 (1)	64.67 (1)	64.80 (2)	64.92 (1)
μ (mm^{-1})	17.98	17.96	17.95	17.91	17.88
Crystal size (mm)	0.14 (radius)	0.14 (radius)	0.14 (radius)	0.14 (radius)	0.14 (radius)
Data collection					
No. of measured, independent and observed [$F > 3.0\ \sigma(F)$] reflections	602, 121, 121	602, 122, 122	602, 118, 118	602, 123, 123	604, 123, 123
R_{int}	0.029	0.029	0.027	0.014	0.018

Table 1 (continued)

T (K)	448	473	498	548	598
$2\theta_{max}$ (°)	120	120	120	120	120
$(\sin\theta/\lambda)_{max}$ (Å^{-1})	1.219	1.219	1.219	1.219	1.219
Refinement					
$R[F > 3\sigma(F)]$, $wR(F)$, S	0.021, 0.025, 1.52	0.021, 0.024, 1.47	0.025, 0.024, 1.55	0.008, 0.008, 1.28	0.016, 0.015, 1.38
No. of reflections	121	122	118	123	123
No. of parameters	6	6	6	6	6

T (K)	648	698	748	778
Crystal data				
Crystal system, space group	Cubic, $Pm\bar{3}m$	Cubic, $Pm\bar{3}m$	Cubic, $Pm\bar{3}m$	Cubic, $Pm\bar{3}m$
a (Å)	4.0221 (1)	4.0248 (2)	4.0273 (2)	4.0286 (1)
V (Å^3)	65.07 (3)	65.20 (4)	65.32 (1)	65.38 (1)
μ (mm^{-1})	17.84	17.80	17.77	17.75
Crystal size (mm)	0.14 (radius)	0.14 (radius)	0.14 (radius)	0.14 (radius)
Data collection				
No. of measured, independent and observed $[F > 3.0\ \sigma(F)]$ reflections	605, 124, 124	605, 125, 125	605, 123, 123	605, 112, 112
R_{int}	0.016	0.017	0.018	0.015
$2\theta_{max}$ (°)	120	120	120	120
$(\sin\theta/\lambda)_{max}$ (Å^{-1})	1.219	1.219	1.219	1.219
Refinement				
$R[F > 3\sigma(F)]$, $wR(F)$, S	0.008, 0.008, 1.29	0.008, 0.008, 1.29	0.011, 0.011, 1.34	0.011, 0.008, 1.34
No. of reflections	124	125	123	112
No. of parameter	6	6	6	6

attempted during the refinements, and the isotropic correction of Type I (Becker & Coppens, 1974*a*,*b*) with a Lorentzian mosaic spread distribution model yielded the best fits.

Alternative indexings of hkl or $hk\bar{l}$ are possible because of the non-centrosymmetric structure of the tetragonal phase (Yoshiasa *et al.*, 1986, 1987). The correct choice was decided based on a comparison of the final R-factors for both cases. The difference in the R-factors between the alternative indexings was 0.2% for the 300 K data.

The atomic positions of $BaTiO_3$ are expressed as follows: Ba (0,0,0), Ti (0.5, 0.5, 0.5), O (0.5, 0.5, 0) for the cubic phase; Ba (0, 0, z), Ti (0.5, 0.5, z), O1 (0.5, 0.5, z), O2 (0.5, 0, z) for the tetragonal phase. In the latter, the Ba site was selected as the origin in the non-centrosymmetric space group $P4mm$, and its z-coordinate was fixed at 0 during the structure refinements. The structure refinements at each temperature converged smoothly to $R = 0.0076$–0.0268 and $R_w = 0.0075-0.0326$ for the anisotropic displacement model. Experimental features and the structure refinement details are summarized in Table 1.

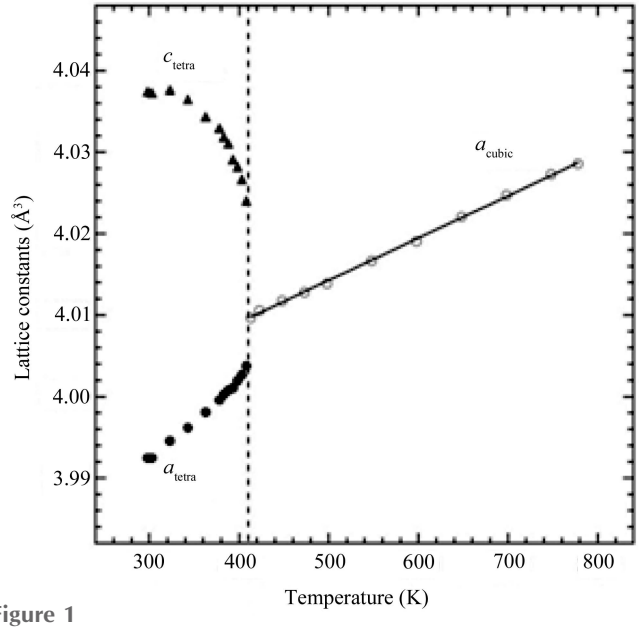

Figure 1
Temperature dependence of the lattice constants of the present $BaTiO_3$. The dotted line hereinafter represents the phase transition point (413 K) from the tetragonal ($P4mm$) to the cubic ($Pm\bar{3}m$) phase.

3. Results and discussion

3.1. Temperature dependence of the lattice constants and volumes

The temperature dependence of the lattice constants, the axial ratio c/a and the lattice volumes are shown in Figs. 1, 2 and 3, respectively. In the tetragonal phase, the a-axis expands, the c-axis shrinks and consequently c/a decreases continuously with increasing temperature. These tendencies change drastically at 413 K; namely, the a- and c-axes lengths agree at 413 K and the c/a ratios continue to keep to unity at this temperature and above. Such a change is also observed in the lattice volumes. These drastic discontinuous changes correspond to the phase transition from the tetragonal ($P4mm$) to the cubic ($Pm\bar{3}m$) phase reported by many researchers. The tetragonal–cubic phase transition temperature of $BaTiO_3$ is known to

differ with the synthetic methods of the crystals, and the reported values vary between 393 and 413 K. In the present $BaTiO_3$ single crystal, the phase transition temperature is determined to be 413 K when the discontinuous changes just occur.

3.2. Structure changes in $BaTiO_3$ with temperature and polarization in ferroelectric phase

Fig. 4 shows the temperature dependence of Δz [$= z_t - z_c$], where z_t and z_c are the z-coordinates of the corresponding atoms in the tetragonal and cubic phases, respectively. Evans (1951, 1961) first showed using X-ray diffraction that in the tetragonal phase the Ti atoms shift slightly along the c-axis from the central positions in the octahedra. The ferroelectricity observed in the tetragonal phase has been discussed based only on such displacements of the Ti atoms. The present Δz value of the Ti atom is 0.0102 (9) at 298 K. This value agrees with those previously reported [Δz = 0.0135 (4) at 301 K from single-crystal X-ray diffraction (Harada *et al.*, 1970); Δz = 0.010 (10) at 298 K from single-crystal neutron diffraction (Buttner & Maslen, 1992)].

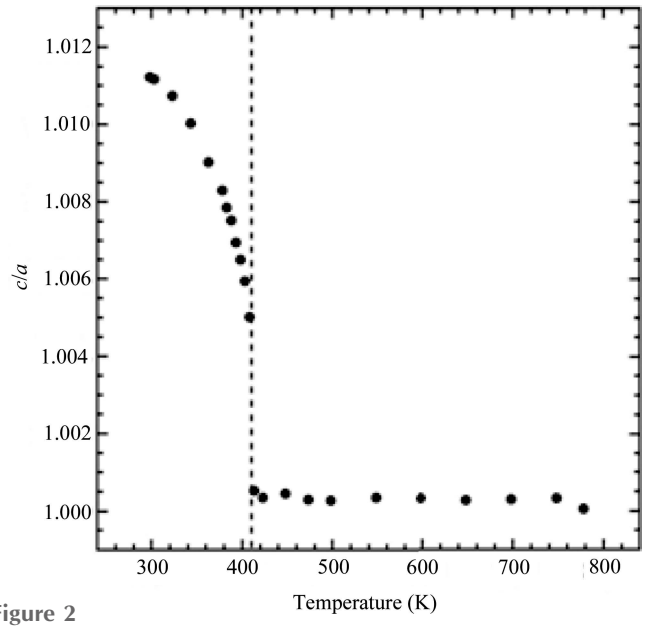

Figure 2
Temperature dependence of the c/a axial ratio in the present $BaTiO_3$.

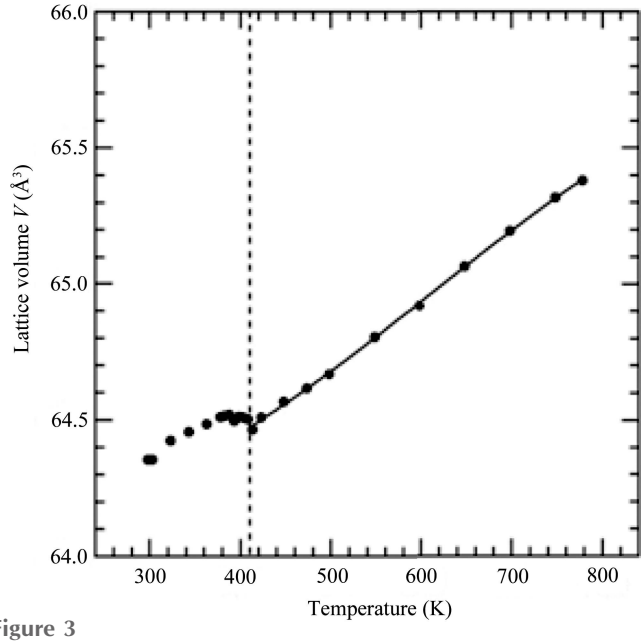

Figure 3
Temperature dependence of the lattice volume in the present $BaTiO_3$.

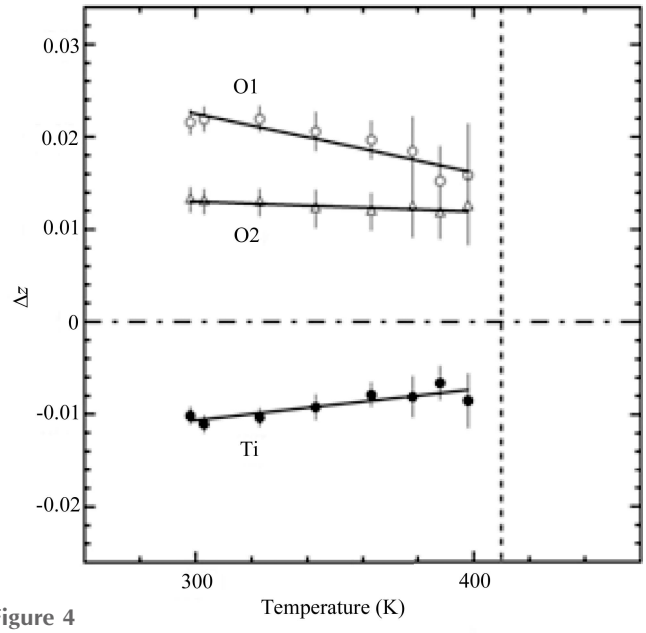

Figure 4
Temperature dependence of the differences (Δz) between atomic positions in the tetragonal and cubic phases. The origin in the non-centrosymmetric space group *P4mm* was set at the Ba site.

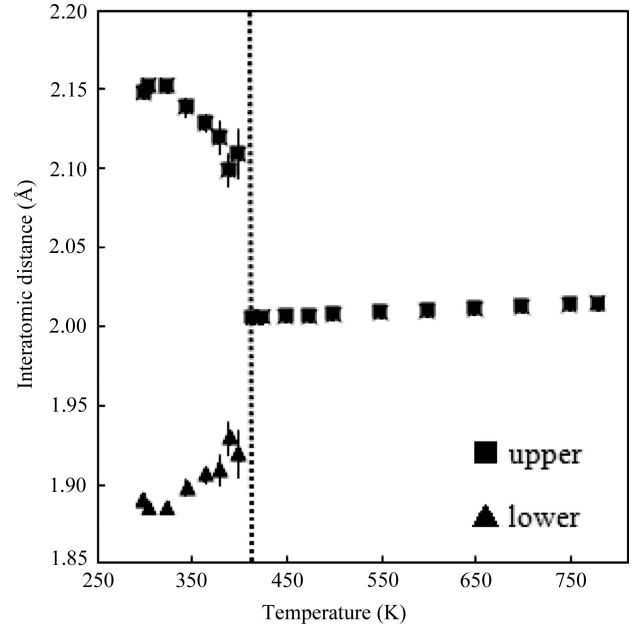

Figure 5
Temperature dependence of the longer and shorter Ti—O1 distances in the TiO_6 octahedron.

As shown in Fig. 4, in the tetragonal phase the Δz values are negative for Ti and positive for O1 and O2. This indicates that the cation (Ti) and the anions (O1, O2) are displaced along the *c*-axis in opposite directions with regard to the Ba positions, set as the origin of the unit cell. The temperature dependence of Δz differs among the atoms. The Δz value of Ti and O1 gradually approaches zero with increasing temperature. The Δz value of O2 depends little on temperature. From these trends, the large Δz components of these atoms are likely to remain just to the vicinity of the phase transition point. The discontinuous and drastic changes of Δz at the transition point can thus be inferred for Ti, O1 and O2. Many researchers have discussed the ferroelectricity based only on the displacement of the Ti atom. However, we should note that the Δz values reflect the relative positional relation along the *c*-axis between Ba, which in fact has a degree of freedom in the *z*-coordinate, and the remaining atoms. Δz involves the actual displacement of Ba as well, so that the discontinuous change is also likely to be present in Ba. The Ba position is, therefore, expected to contribute to polarization as well as the Ti position (Fig. 4).

Figs. 5 and 6 show the temperature dependence of Ti—O1 and Ba—O2 bond distances. The difference between the longer and shorter Ti—O1 bond distances is 0.257 Å at 303 K, which is 10% larger than the average Ti—O1 distance. The difference between the longer and shorter Ba—O2 bond distances is 0.075 Å (less than 3% of the average Ba—O2 distance). The differences show that Ti and Ba occupy off-center positions in TiO_6 and BaO_{12} polyhedra, respectively. The difference between the longer and shorter Ti—O1 bond distances obviously decreases with increasing temperature. This shows that the distortion of the TiO_6 octahedron decreases and Ti moves from an off-center position to a central position in the octahedron with increasing temperature towards the phase transition point. The same behavior is also clearly observed in the Ba—O2 distances. After the discontinuous and drastic changes of Ti—O1 and Ba—O2 bond distances with the transition to the cubic phase, both distances increase linearly with increasing temperature. Although the Ti atom statistically occupies the ideal octahedral position stabilized by thermal vibration, the local positional distortion around the Ti site may remain. Such a situation may also occur in the Ba site.

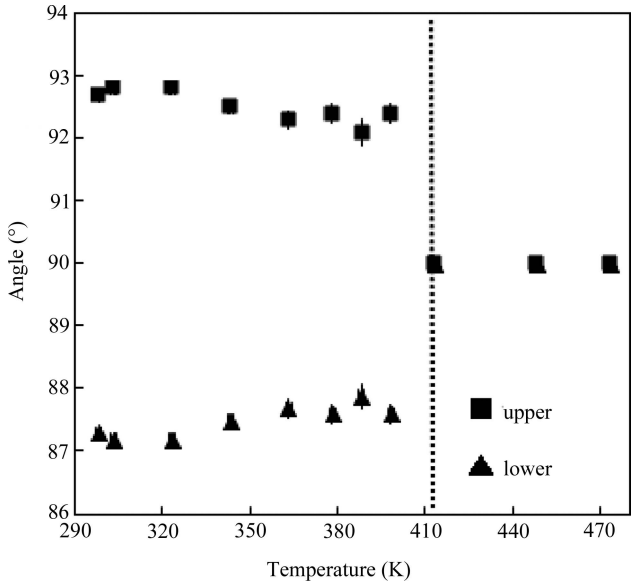

Figure 7
Temperature dependence of the larger and smaller O1—Ti—O2 angles in the TiO_6 octahedron.

Figs. 7 and 8 show the temperature dependence of the O1—Ti—O2 angles and O1—O2 distances in the TiO_6 octahedron, respectively. In the tetragonal phase, the difference between

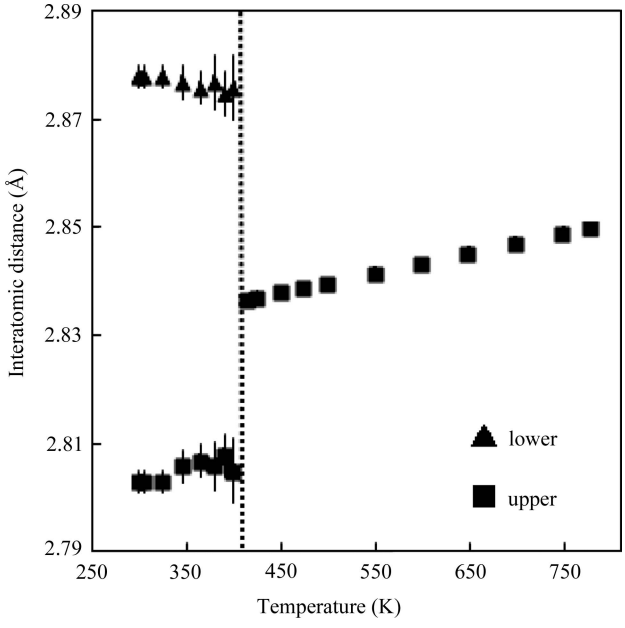

Figure 6
Temperature dependence of the longer and shorter Ba—O2 distances in the TiO_6 octahedron.

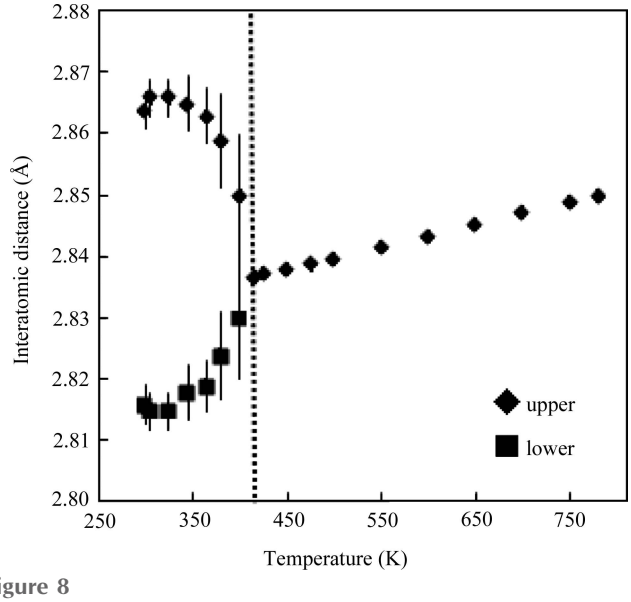

Figure 8
Temperature dependence of the longer and shorter O1—O2 distances in the TiO_6 octahedron.

larger and smaller O1—Ti—O2 angles only shows a gradual decrease with increasing temperature, and it is kept at $\sim 5^\circ$ up to the phase transition point (Fig. 7). After that, at the phase transition point a discontinuous change is observed in the O1—Ti—O2 angles, as well as in Ti—O1 (Fig. 5) and Ba—O2 (Fig. 6). This discontinuous change at the phase transition point implies that a component of local distortion (off-center position) in the polyhedral sites of cations remains even in the high-temperature cubic phase, and this effect is especially predominant around the Ti site with larger distortion. In contrast, the difference between longer and shorter O1—O2 bond distances has a value of 0.05 Å at 303 K, which is less than 2% of the average O1—O2 distance (Fig. 8). This difference rapidly decreases with increasing temperature, especially near the phase transition point. This implies that the O1—O2 distances have a continuous variation at the phase transition point, as in the lattice volume (Fig. 3). Such continuous variation of larger oxygen–anion distances contributes to that of the lattice volume.

3.3. Temperature dependence of mean-square displacements and origin of ferroelectricity

Fig. 9 shows the temperature dependence of the equivalent isotropic temperature factors U_{eq} for each atom. The temperature factors U_{eq} obtained from diffraction analyses include the effects of static and dynamic disorders. The static disorder is the configurational disorder, while the dynamic disorder arises from the thermal vibration of atoms. The values will follow straight lines and pass through the origin by classical statistical dynamics if the effect of configurational disorder is negligible (Willis & Pryor, 1975). The effect of configurational disorder is divided from dynamic effects by the temperature dependence of U_{eq} and can be estimated from the 0 K intercept of the straight line (Yoshiasa *et al.*, 1987; Nakatsuka *et al.*, 2011). When the static distribution is present, the straight line does not pass through the origin and the 0 K intercept has a positive value. A steeper gradient shows that effective potential is softer. In the cubic phase, it becomes softer in the order Ti < Ba < O (Fig. 9). All lines can be extrapolated to the value zero at 0 K, except for the straight line for U_{eq}(Ti) in the cubic phase (Figs. 9 and 10). In the tetragonal crystals, there is no experimental observation of configurational disorder. This result does not support the conclusions of Comès *et al.* (1968), who proposed a statistical distribution for all the atoms. The straight line for U_{eq}(Ti) in the cubic phase deviates significantly from the origin. This suggests strongly that Ti includes the clear configurational disorder (statistical distribution) effect only in the cubic phase. The Ti atoms occupy the off-center positions in TiO_6 octahedra, whereas the static distribution cannot clearly be observed for Ba and O atoms.

The 0 K intercept value of 0.0023 Å^2 is estimated by the straight line for U_{eq}(Ti) in the cubic phase (Fig. 10). The calculated root-mean-square value is about 0.047 Å in length. It can be estimated from Fig. 4 that the displacement in z-coordinates of Ti from the Ba position (z = 0.0) in the tetragonal phase around the phase transition point is 0.0078 Å. This displacement corresponds to the distance of 0.044 Å, which is close to the value of 0.047 Å mentioned above. Figs.

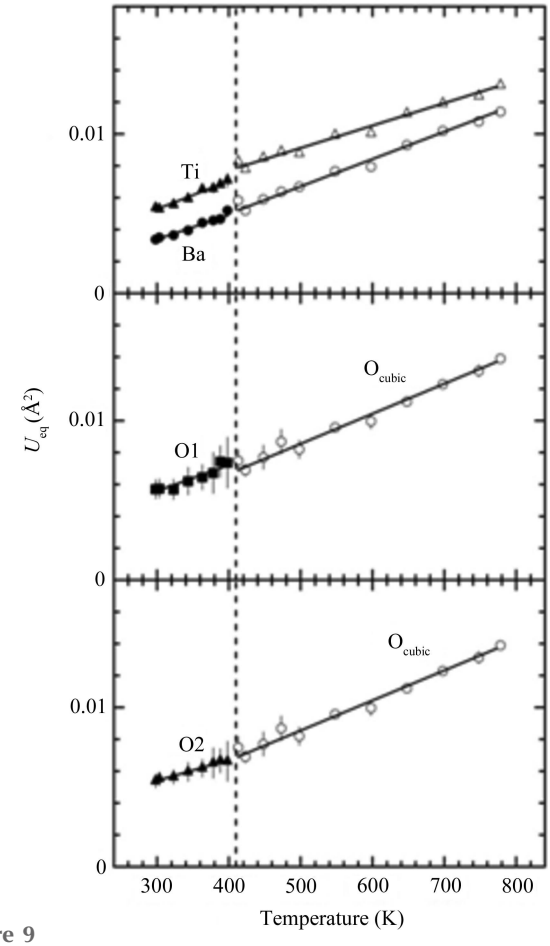

Figure 9
Temperature dependence of U_{eq} for each atom. Sizes of error bar are smaller than the circle, triangle and square marks.

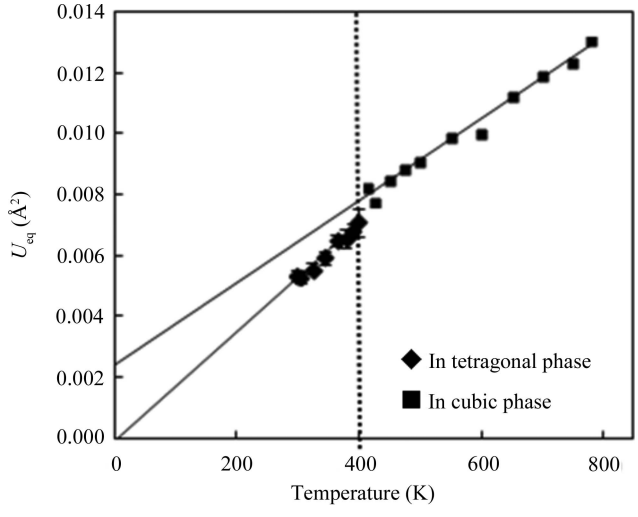

Figure 10
Extrapolation of the temperature dependence of U_{eq} for Ti atoms. The sizes of the error bars are smaller than the circle, triangle and square marks.

11(*a*) and (*b*) show three-dimensional electron density distributions and a difference Fourier map through the Ti position and parallel to the (001) plane. Large positive residual electron density peaks are observed toward the [100] and [010] directions representing the Ti static disorder. It seems that the relationship in the spatial distributions of Ti and Ba in the tetragonal phase is maintained in the cubic phase and the interaction of Ti and Ba is presumed. Although we tried split-atom models for the cubic phases, the Ti position did not converge on the split-atom position but converged on the average on-center position. The U_{eq} value for Ti at 398 K in the tetragonal phase without statistical distribution is 0.0071 (5) Å^2 and the root-mean-square value is 0.084 Å for the thermal vibration amplitude. In the cubic phase at higher temperature, the root-mean-square value of 0.047 Å by configurational displacement of 0.0023 Å^2 is about half the thermal vibration amplitude. Therefore, split-atom models were not suitable for the cubic system. Although many models have been proposed for the tetragonal and cubic phases (Comès *et al.*, 1968, 1970; Itoh *et al.*, 1985; Tkacz-Śmiech *et al.*, 2003), they all disagree in many respects with the single domain crystal structure analyses (Harada *et al.*, 1970; Buttner & Maslen, 1992) in many respects. It is important that configurational disorder is not observed in particular in the tetragonal phase. The evidence of the statistical distribution toward the body-diagonal direction of Ti is not observed at all. The proposed models (Comès *et al.*, 1968, 1970; Itoh *et al.*, 1985; Tkacz-Śmiech *et al.*, 2003) should be re-examined.

In summary, the Ti atoms in the tetragonal phase are located at the off-center positions of the TiO_6 octahedra without statistical distribution and its ferroelectricity originates basically in the displacive type. The difference between the longer and shorter Ti—O1 bond distances reaches 0.27 Å at 298 K, and then obviously decreases toward the phase transition point. The displacement magnitude is large, and is clearly visible in Fig. 12(*a*). The Ti atoms are statistically distributed around the off-center positions of regular TiO_6 octahedra in the cubic phase (configurational disorder), as shown in Fig. 12(*b*). The order–disorder component in the

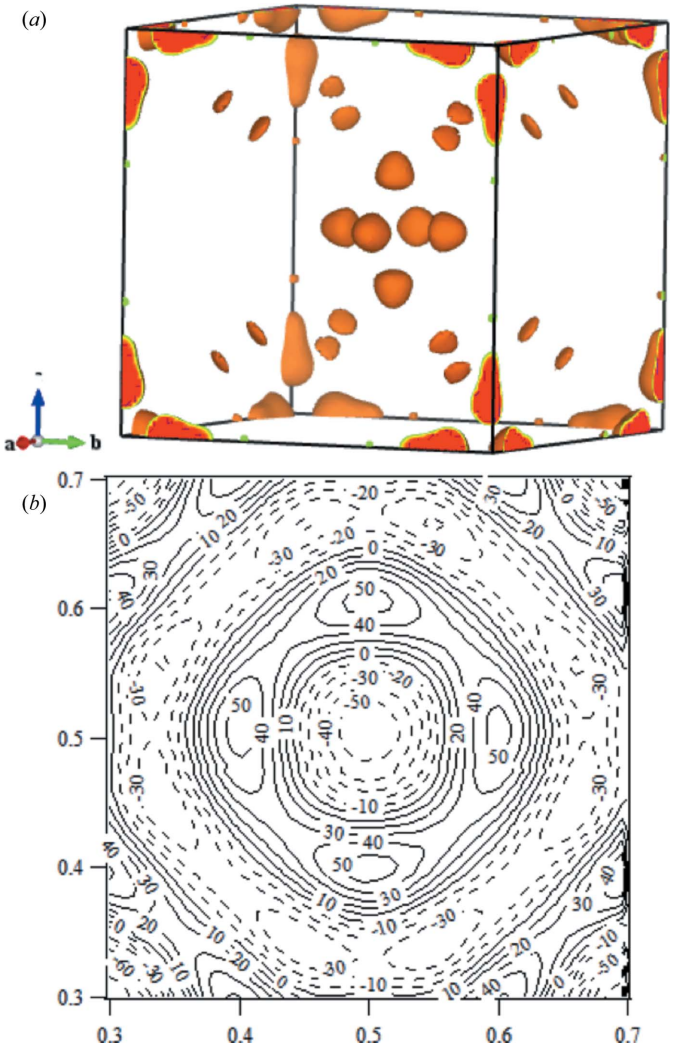

Figure 11
(*a*) Three-dimensional electron-density distribution in the cubic phase calculated by Fourier transform. (*b*) The section of the difference-Fourier map on the (001) plane at z = 0.5 in the cubic phase. The electron densities are multiplied by 100 and the contour intervals are 10 e Å^{-3}. Positive and negative contours are solid and dashed lines, respectively.

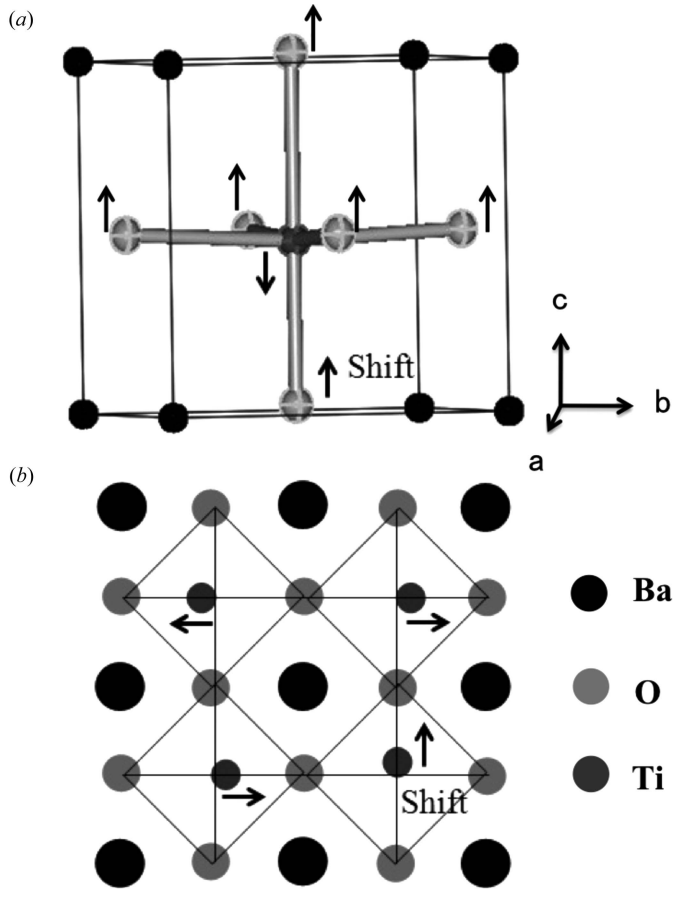

Figure 12
(*a*) The crystal structure of the tetragonal $BaTiO_3$ phase at 298 K (displacement ellipsoids are drawn at the 90% probability level). (*b*) Schematic view of the static displacements of Ti atoms in the cubic phase. The magnitude of displacement was estimated as 0.047 Å in the [001] direction.

cubic phase is essentially mainly from static displacements of Ti atoms.

Acknowledgements

This study was performed under the auspices of the Photon Factory (PAC No. 2009G049).

References

Becker, P. J. & Coppens, P. (1974*a*). *Acta Cryst.* A**30**, 129–147.
Becker, P. J. & Coppens, P. (1974*b*). *Acta Cryst.* A**30**, 148–153.
Buttner, R. H. & Maslen, E. N. (1992). *Acta Cryst.* B**48**, 639–644.
Comès, R., Lambert, M. & Guinier, A. (1968). *Solid State Commun.* **6**, 715–719.
Comès, R., Lambert, M. & Guinier, A. (1970). *Acta Cryst.* A**26**, 244–254.
Danner, H. R., Frazer, B. C. & Pepinsky, R. (1960). *Acta Cryst.* **13**, 1089.
Evans, H. T. (1951). *Acta Cryst.* **4**, 377.
Evans, H. T. (1961). *Acta Cryst.* **14**, 1019–1026.
Frazer, B. C., Danner, H. R. & Pepinsky, R. (1955). *Phys. Rev.* **100**, 745–746.
Harada, J., Pedersen, T. & Barnea, Z. (1970). *Acta Cryst.* A**26**, 336–344.
Itoh, K., Zeng, L. Z., Nakamura, E. & Mishima, N. (1985). *Ferroelectrics*, **63**, 29–37.
Megaw, H. D. (1945). *Nature (London)*, **155**, 484–485.
Megaw, H. D. (1946). *Proc. Phys. Soc.* **58**, 133–152.
Megaw, H. D. (1947). *Proc. R. Soc. London Ser. A*, **189**, 261–283.
Miyanaga, T., Diop, D., Ikeda, S. I. & Kon, H. (2002). *Ferroelectics*, **274**, 41–53.
Nakatsuka, A., Shimokawa, M., Nakayama, N., Ohtaka, O., Arima, H., Okube, M. & Yoshiasa, A. (2011). *Am. Mineral.* **96**, 1593–1605.
Ravel, B. & Stern, E. A. (1995). *Physica B Condens. Matter*, **208–209**, 316–318.
Revel, B., Stern, E. A., Vedrinskii, R. I. & Kraizman, V. (1998). *Ferroelectrics*, **206**, 407–430.
Rhodes, R. G. (1949). *Acta Cryst.* **2**, 417–419.
Sasaki, S. (1987). *RADY*. National Laboratory for High Energy Physics, Japan.
Sicron, N., Ravel, B., Yacoby, Y., Stern, E. A., Dogan, F. & Rehr, J. J. (1994). *Phys. Rev. B*, **50**, 168–180.
Tanaka, K. & Lehmpfuhl, G. (1972). *Jpn. J. Appl. Phys.* **11**, 1755–1756.
Tkacz-Śmiech, K., Koleżyński, A. & Ptak, W. S. (2003). *Solid State Commun.* **127**, 557–562.
Tokonami, M. (1965). *Acta Cryst.* **19**, 486.
Willis, B. T. M. & Pryor, A. W. (1975). *Thermal Vibrations in Crystallography*. Cambridge University Press.
Wilson, A. J. C. (1992). Editor. *International Tables for Crystallography*, Vol. C. Dordrecht: Kluwer Academic Publishers.
Yoshiasa, A., Koto, K., Kanamaru, F., Emura, S. & Horiuchi, H. (1987). *Acta Cryst.* B**43**, 434–440.
Yoshiasa, A., Ueno, K., Kanamaru, F. & Horiuchi, H. (1986). *Mater. Res. Bull.* **21**, 175–181.